




Comparative analysis of folding and unfolding dynamics and free-energy landscapes in homologous cold shock proteins with variable thermal stabilities

Zhenyong Xue,^{1,2} Hao Sun ^{1,2} Haiyan Hong,¹ Zhuwei Zhang,^{1,2} Yuhang Zhang ^{1,2} Zilong Guo,² Shimin Le,^{1,*} and Hu Chen ^{1,2,†}

¹Research Institute for Biomimetics and Soft Matter, Fujian Provincial Key Lab for Soft Functional Materials Research, Department of Physics, Xiamen University, Xiamen 361005, China

²Center of Biomedical Physics, Wenzhou Institute, University of Chinese Academy of Sciences, Wenzhou 325000, China



(Received 10 January 2024; accepted 1 May 2024; published 14 May 2024)

Cold shock proteins from the mesophilic organism *Bacillus subtilis* (BsCSP), the thermophilic organism *Bacillus caldolyticus* (BcCSP), and the hyperthermophilic organism *Thermotoga maritima* (TmCSP) are homologous proteins with similar native structure but quite different thermal stabilities, which makes them promising candidates for investigating the general and specific aspects the folding and unfolding dynamics of proteins and free-energy landscapes. In this study, we employed magnetic tweezers to explore the force-dependent folding and unfolding rates of BsCSP, BcCSP, and TmCSP at forces from several pN to tens of pN. Our results indicate similar force-dependent folding rates for these three proteins, while the unfolding rate of BsCSP, BcCSP, and TmCSP decreases sequentially, consistent with previous biochemical findings. Comparing with TmCSP, BcCSP shows lower but sufficient stability with folding free energy of $8.0 k_B T$, and its force-dependent unfolding rates exhibit tremendous nonlinear behavior deviated from Bell's model like TmCSP. BsCSP has very low stability with folding free energy of only $3.9 k_B T$, and its force-dependent unfolding rates at 3–10 pN exhibit almost linear behavior. Comprehensive free-energy landscapes are constructed, revealing common barriers that governs folding and unfolding dynamics for BcCSP and TmCSP but a wide merged barrier for BsCSP. Our findings provide valuable insights into the folding and unfolding mechanisms of these CSPs, shedding light on the relationship between protein structure, stability, and mechanical properties.

DOI: [10.1103/PhysRevResearch.6.023170](https://doi.org/10.1103/PhysRevResearch.6.023170)

I. INTRODUCTION

Most proteins adopt unique, three-dimensional native structures determined by their specific amino acid sequences. Previous research has shown that the folding rates of single-domain proteins correlate with topological features of their native states [1–4]. Two key properties that enable proteins to achieve and maintain their native structures are the kinetic capability to fold rapidly and the thermodynamic stability of the folded state. Structural homologous proteins with similar three-dimensional structures can have different thermal stability [5,6]. Therefore, they are ideal objects to study the effect of thermal stability on the folding and unfolding dynamics of proteins.

Homologous proteins from mesophilic, thermophilic, and hyperthermophilic bacteria exhibit increasing thermal stability that associated with an increased number of salt bridges [7–13], enhanced packing density [11], amplified

hydrophobicity [12–15], and diminished loop or flexible regions within these proteins [16,17]. Homologous cold shock proteins (CSPs), prevalent in numerous bacteria, play a pivotal role in responding to swift temperature declines. Serving as nucleic acid chaperones [18–21], CSPs can inhibit the formation of secondary mRNA structures at low temperatures, thereby facilitating the initiation of translation. CSPs are compact proteins without disulfide bonds or tightly bound cofactors [22], which makes them proper to study protein folding dynamics. CSPs from the mesophilic organism *Bacillus subtilis* (BsCSP), the thermophilic organism *Bacillus caldolyticus* (BcCSP), and the hyperthermophilic organism *Thermotoga maritima* (TmCSP) have highly conservative native structure and very different thermal stabilities. They all form a β -barrel structure with five antiparallel β strands arranged in two β sheets (Fig. 1, top) [23,24]. Sequence alignment of CSPs, BcCSP differs from BsCSP in 12 locations (including a deletion at the C terminus), while TmCSP differs from BsCSP in 24 locations (including three deletions, one insertion and one additional residue at the C terminus). The numbers of charged residues of BsCSP, BcCSP, and TmCSP are 19, 17, and 24, respectively (Fig. 1, bottom).

Backbone C_α root-mean-square displacements between BsCSP and BcCSP, BsCSP and TmCSP, and BcCSP and TmCSP are 0.6, 1.2, and 1.2 angstroms, respectively. The thermal stability of BsCSP, BcCSP, and TmCSP is enhanced successively, and their melting temperatures are 50° , 72° , and 85°C , respectively [25].

*leshimin@xmu.edu.cn

†chenhu@xmu.edu.cn

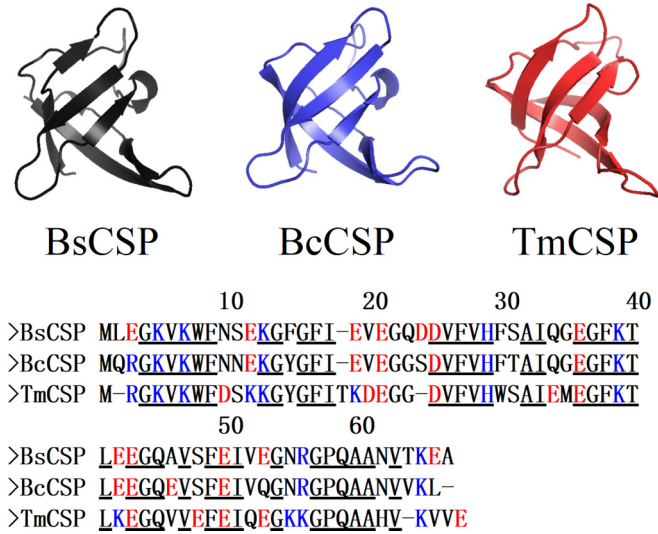


FIG. 1. The native structures and amino acid sequences of BsCSP, BcCSP, and TmCSP. Among the amino acid sequences, negative charged ones are marked in red, while positive charged ones are marked in blue. Conserved amino acids are underlined.

Previous biochemical experiments on these three CSPs used guanidine hydrochloride (GdmCl) to unfold proteins and analyzed the conformation transition by measuring changes in tryptophan fluorescence intensity during denaturation and renaturation [25]. In the absence of GdmCl, the rate constants of unfolding k_{NU} for BsCSP, BcCSP, and TmCSP are 9.93, 0.64, and 0.018 s^{-1} , respectively, and folding rates k_{UN} are 689, 1370, and 565 s^{-1} , respectively. The results indicate that CSPs are typical two-state proteins and the large difference in stability among CSPs is reflected in the unfolding rate rather than the folding rate.

In single molecular experiments, TmCSP has been investigated by traditional constant-pulling-speed atomic force microscopy (AFM), force-clamp AFM, and magnetic tweezers [26–28]. Multiple intermediate states were observed in force-clamp AFM, and both traditional AFM and magnetic tweezers experiments demonstrate TmCSP has two-state unfolding behavior with a single-step transition. In comparison to AFM, magnetic tweezers can maintain constant force for a long time without the need for a feedback system [29–33]. In magnetic tweezers experiments, the equilibrium folding and unfolding dynamics near the critical force of 6.6 pN yielded a folding free energy of $12.6 k_B T$. It was also found that the unfolding rate shows different force sensitivity at force ranges above 8 pN and below 8 pN, which gives a free-energy landscape with two barriers [28].

Here we explored the force-dependent folding and unfolding dynamics of all three types of CSPs (BsCSP, BcCSP, and TmCSP) by magnetic tweezers. Consistent with the biochemical findings, the force-dependent folding rates are similar for BcCSP and TmCSP, with BsCSP slightly lower. On the other hand, the mechanical hierarchy of CSPs to resist unfolding from the strongest to the weakest is TmCSP > BcCSP > BsCSP. The force-dependent unfolding rates of BcCSP and TmCSP exhibit remarkable different force responses in low and high force regimes, while those of BsCSP shows almost linear

force sensitivity. Based on the measured force-dependent folding and unfolding rates, we constructed the free-energy landscapes of CSPs and discussed their shared characteristics and specific properties.

II. MATERIALS AND METHODS

A. Protein construct preparation

The recombinant protein constructs $6 \times \text{His-AviTag-I27}_2\text{-CSP-I27}_2\text{-SpyTag}$ were created by inserting gene sequences of three Csp, which were synthesized by GenScript Biotech, into the vector pET151-I27₄ which contains two Titin-I27 domains on each side of their multiple cloning sites (Fig. S1) [41]. To produce biotinylated proteins, plasmids of pET151 and pBirA (biotin ligase expression plasmid) were transformed into the *Escherichia coli* strain BL21 (DE3). The selected transformant on LB plates was cultured in LB medium supplemented with chloramphenicol, ampicillin, and D-biotin at 37°C until the optical density of the bacterial cells reached 0.6. Protein expression was induced by adding 0.5 mM isopropyl β -D-thiogalactopyranoside and incubating for 12 h at 25°C . The cells were harvested by centrifugation and lysed by sonication in a buffer containing 50 mM Tris, 500 mM NaCl, 10% glycerol, 5 mM imidazole, 5 mM 2-mercaptoethanol, and pH 8.0. The target proteins were purified using Ni-NTA Sefinose resin (Sangon Biotech) and Superdex 200 (GE Healthcare) following the manufacturer’s protocol. Finally, the protein was snap-frozen in liquid nitrogen and stored at -80°C .

B. Sample preparation for magnetic tweezers

The coverslips were cleaned in detergent solution and DI water by ultrasonic and oxygen plasma cleaner and then put in a solution of 1% 3-aminopropyltriethoxy-silane (APTES, cat. A3648, Sigma) in methanol for 50 min. A flow chamber was created by sandwiching a parafilm between the APTES-coated coverslip and another piece of cleaned coverslip. Microspheres (cat. 417145, Polysciences) with a diameter of 3 μm were flushed and incubated for 15 min to attach to the coverslip surface. The chamber was flushed with 1% Sulfo-SMCC (SE 247420, Thermo Science) in $1 \times \text{PBS}$ and incubated for 25 min. Subsequently, the SpyCatcher protein with N-terminal cysteine was flushed into the chamber and incubated for 1.5 h. To block nonspecific interactions, 1% BSA in $1 \times \text{PBS}$ was added to the chamber and stored overnight at 4°C . Then CSP protein construct was flushed into the chamber and incubated for 20 min. Following that, streptavidin-coated paramagnetic beads (Dynabead M270) were flushed into the chamber to form protein tethers for magnetic tweezers experiments.

The homemade magnetic tweezers were built around an inverted microscope that utilized double antiparallel magnetic rods to apply stretching forces on proteins for studying their force-dependent folding and unfolding dynamics. For detailed design information regarding the magnetic tweezers, please refer to our previous publication [30,34].

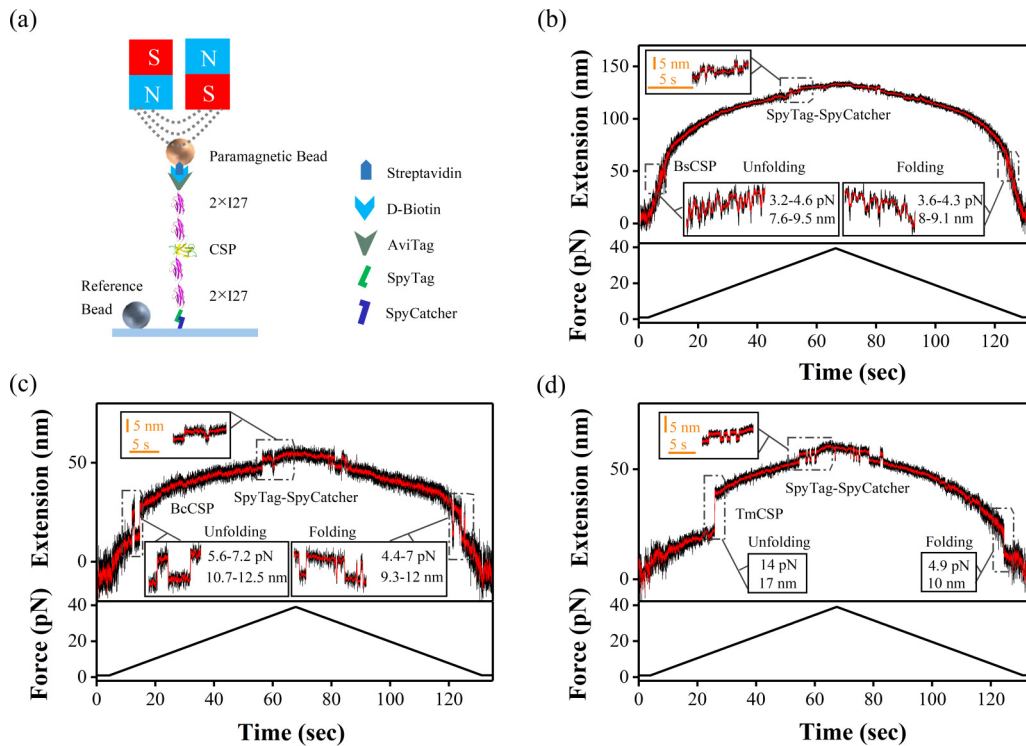


FIG. 2. Diagram of the protein construct in magnetic tweezers experiment and the representative extension time courses in constant loading rate experiment. (a) Schematic of magnetic tweezers stretching protein construct of AviTag(biotin)-I27₂-CSP-I27₂-SpyTag which was attached to a streptavidin-coated paramagnetic bead and SpyCatcher-coated coverslip surface. CSP represents the three types of CSPs studied in this paper. [(b)–(d)] Extensions of CSP protein constructs were recorded (top panel) when force increased with a loading rate of 0.6 pN/s from 1 to 39 pN and decreased with loading rate -0.6 pN/s from 39 to 1 pN (bottom panel). (b) When force was increasing, BsCSP unfolded with step size of 7.6 nm at ~ 3.2 pN, then refolded and unfolded several times. The last unfolding event occurred with step size of 9.5 nm at ~ 4.6 pN. When force was decreasing, a refolding step with step size of 9.1 nm was observed at ~ 4.3 pN, then unfolded and folded several times. The last folding event occurred with step size of 8 nm at ~ 3.6 pN. (c) When force was increasing, BcCSP unfolded with step size of 10.7 nm at ~ 5.6 pN, then refolded and unfolded again with step size of 12.5 nm at ~ 7.2 pN. When force was decreasing, a refolding step with step size of 12 nm was observed at ~ 7 pN, then unfolded and folded several times. The last folding event occurred with step size of 9.3 nm at ~ 4.4 pN. (d) When force was increasing, TmCSP unfolded with step size of 17 nm at ~ 14 pN. A refolding step with step size of 10 nm was observed at ~ 4.9 pN when force was decreasing. In all experiments, raw data were recorded at 200 Hz (black) and smoothed in time window of 0.1 s (red). The typical fingerprint signal of around 4 nm from SpyTag-SpyCatcher was observed at ~ 30 pN.

III. RESULTS

A. Increasing mechanical stability of BsCSP, BcCSP, and TmCSP

In the magnetic tweezers experiment, we connected the protein construct AviTag(biotin)-I27₂-CSP-I27₂-SpyTag to the superparamagnetic sphere M270 coated with streptavidin and the glass surface covered by SpyCatcher [Fig. 2(a)] [35]. The CSP used was BsCSP, BcCSP, or TmCSP.

To determine the characteristic trajectories of three CSP proteins in force-dependent folding and unfolding, we first stretched each of them with constant loading rate. The CSP tethers were stretched at a loading rate of 0.6 pN/s from 1 to 39 pN and -0.6 pN/s back from 39 to 1 pN. For BsCSP, multiple unfolding and folding steps were observed from ~ 3.2 to ~ 4.6 pN, with step sizes ranging from 7.6 to 9.5 nm. Multiple refolding and unfolding steps were also observed from ~ 3.6 to ~ 4.3 pN, with step sizes ranging from 8 to 9.1 nm when force is decreasing [Fig. 2(b)]. Unfolding of CSP and the four I27 domains could be observed when the force was loaded to 80 pN (Fig. S2) [41].

For BcCSP, multiple unfolding and folding steps were observed from ~ 5.6 to ~ 7.2 pN, with step sizes ranging from 10.7 to 12.5 nm with increasing force. Multiple refolding and unfolding steps were also observed from ~ 4.4 to ~ 7 pN, with step sizes ranging from 9.3 to 12 nm with decreasing force [Fig. 2(c)]. In contrast, for TmCSP, a single unfolding step was observed at ~ 14 pN with a step size of 17 nm, and a single refolding step was observed at ~ 4.9 pN with a step size of 10 nm [Fig. 2(d)]. This is consistent with previous studies [28]. The increasing unfolding and refolding forces observed for BsCSP, BcCSP, and TmCSP are consistent with their increasing thermal stabilities in the same order.

B. Decreasing unfolding rates and similar folding rates of BsCSP, BcCSP, and TmCSP from constant force equilibrium measurement

As the reversible folding and unfolding transitions have been observed at constant loading rate experiments, equilibrium dynamics can be measured when we keep a constant stretching force close to the critical value. We found that the

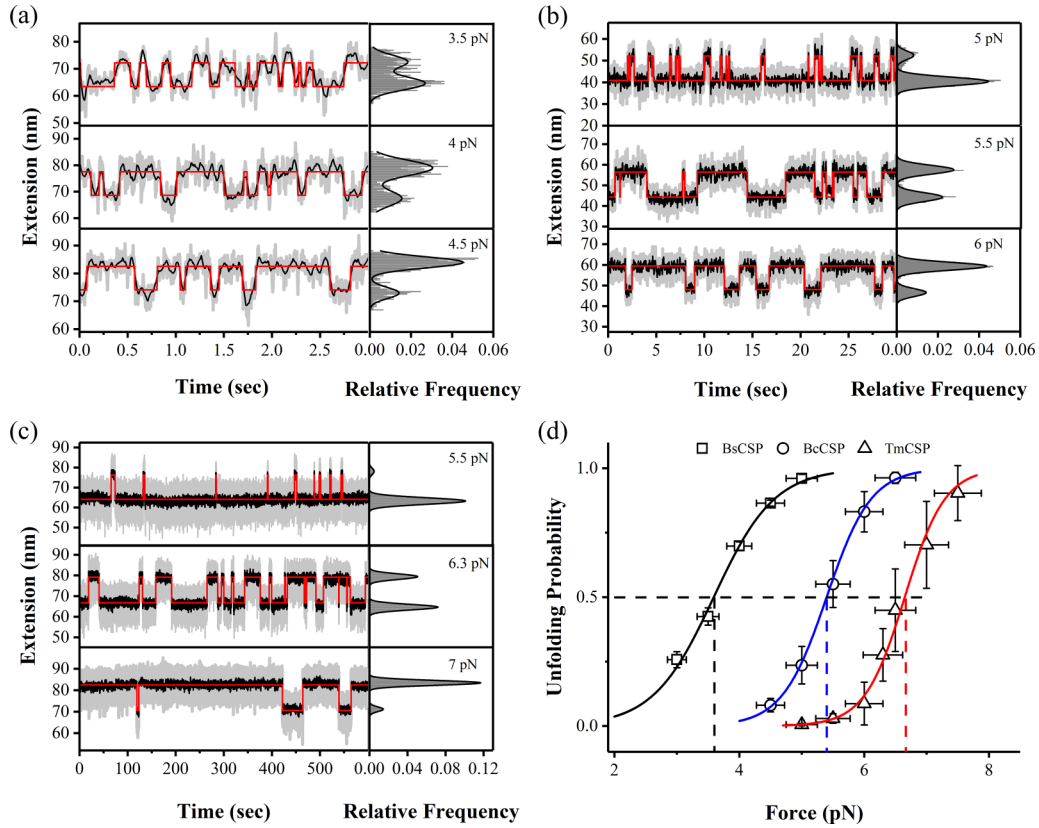


FIG. 3. Equilibrium measurement of three CSPs at constant forces. (a) Extension time course of BsCSP at 3.5, 4.0, and 4.5 pN for 3 s. (b) Extension time course of BcCSP at 5.0, 5.5, and 6.0 pN for 30 s. (c) Extension time course of TmCSP at 5.5, 6.3, and 7.0 pN for 600 s. Raw data were recorded at 200 Hz (gray) and smoothed in a time window of 0.1 s for BsCSP and BcCSP and 0.25 s for TmCSP (black). Red lines show the results of hidden Markov model analysis. The right panel shows corresponding relative frequency of the smoothed extensions and fitting curves by two-peak Gaussian function. (d) Force-dependent unfolding probabilities of three CSPs are fitted by Eq. (1). The average unfolding probabilities of BsCSP, BcCSP were determined from three independent tethers, and those of TmCSP were obtained from five independent tethers. Error bars show the standard deviation, and force is estimated to have 5% uncertainty.

extension jumped back and forth at narrow force ranges from 3 to 5 pN for BsCSP, from 4.5 to 6.5 pN for BcCSP, and from 5 to 7.5 pN for TmCSP, corresponding to the folding and unfolding transitions of CSPs [Figs. 3(a)–3(c)]. Please note that the timescales are different: just 3 s for BsCSP, 30 s for BcCSP, and 600 s for TmCSP because of the huge difference in transition rates. The histogram of the smoothed extension showed two peaks, corresponding to the unfolded state and the native state, which give the average transition step sizes of CSPs at forces close to their respective critical forces. We got average force-dependent probability of unfolding [$P_u(f)$] [Fig. 3(d)] which could be fitted with equation:

$$P_u(f) = \frac{1}{\exp[-(f - f_c)\Delta x/k_B T] + 1}, \quad (1)$$

where f_c denotes the critical force at which $P_u(f_c) = 50%$; Δx the extension changes; k_B Boltzmann constant, and T the absolute temperature. The fitting gives $f_c = 3.6$ pN and $\Delta x = 8.4$ nm for BsCSP, $f_c = 5.4$ pN and $\Delta x = 11.5$ nm for BcCSP. Previous study [28] and our new measurement give $f_c = 6.6$ pN and $\Delta x = 12.7$ nm for TmCSP, which is consistent with the recorded step size [Fig. 3(d)].

The folding and unfolding rates of BsCSP (3.5 and 4.5 pN), BcCSP (5 and 6 pN), and TmCSP (5.5 and 7 pN) were

determined by exponential fitting to the survival probability of folded state and unfolded state of CSPs, respectively [Figs. 4(a), 4(b) and 4(c)]. The force-dependent unfolding rates of BsCSP, BcCSP, and TmCSP sequentially decrease with one to two orders of magnitude. Similarly to TmCSP, the force-dependent unfolding rate of BsCSP from 3 to 5 pN and BcCSP from 4.5 to 6.5 pN can be described by the Bell’s model, $k_u(f) = k_u^0 \exp(fx_u/k_B T)$, where k_u^0 represents the unfolding rate at zero force and x_u corresponds to the unfolding distance. The force-dependent unfolding rates for BsCSP were fitted with Bell’s model, yielding the following parameters (the subscript “2” is for the fitting at low force regime): $k_{u,2}^0 = 1.5 \pm 0.5$ s⁻¹ and $x_{u,2} = 1.7 \pm 0.3$ nm. Similarly, the fitting parameters for BcCSP are as follows: $k_{u,2}^0 = (1.0 \pm 0.6) \times 10^{-2}$ s⁻¹ and $x_{u,2} = 3.5 \pm 0.5$ nm which is close to unfolding distance of TmCSP: $x_{u,2} = 3.1 \pm 0.2$ nm [Fig. 4(d)].

Compared to the force-dependent unfolding rates, the folding rates of CSPs demonstrate higher sensitivity to force. The folding rates of BcCSP and TmCSP align with a shared curve, while BsCSP has slightly lower folding rates, represented by a separate curve [Fig. 4(d)]. Approximately, we consider the transition state of protein as a solid body, and only its orientation fluctuation changes its extension $x_{ts}(f)$ in the direction of

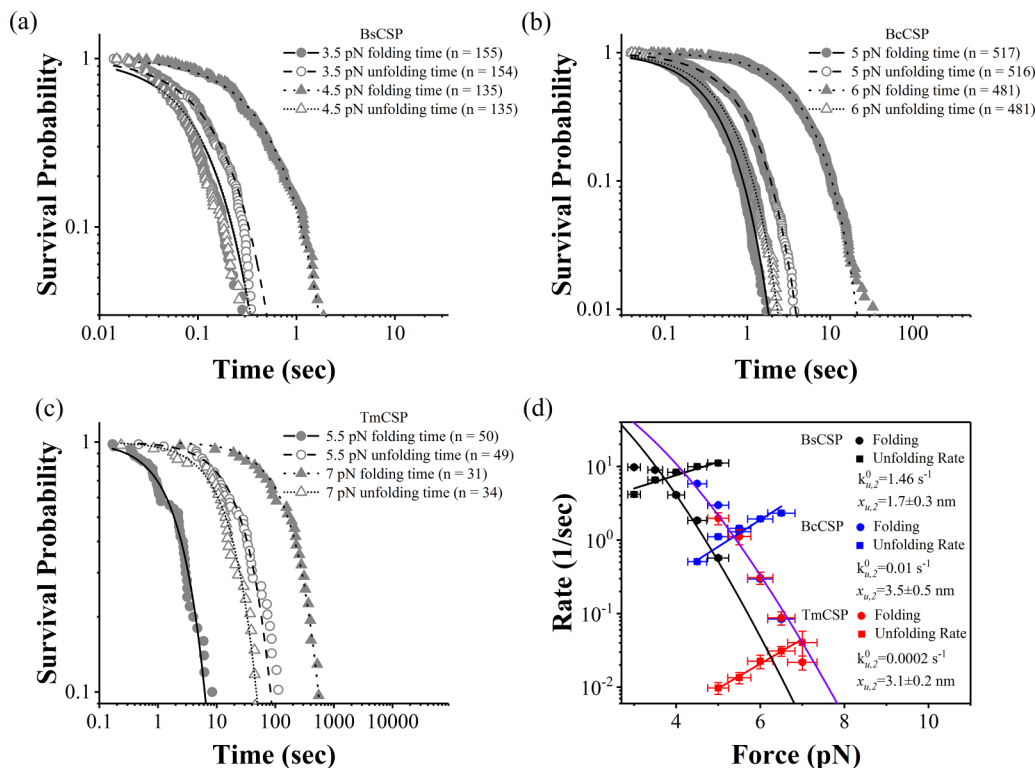


FIG. 4. Folding and unfolding rates obtained from equilibrium constant force measurement of three CSPs. [(a)–(c)] The survival probability of native states and unfolded states of BsCSP at 3.5 and 4.5 pN (a), BcCSP at 5 and 6 pN (b), and TmCSP at 5.5 and 7 pN (c). The lines are exponential fitting results to determine k_u and k_f . (d) The average unfolding and folding rates were obtained from equilibrium constant force measurement for three independent BsCSP, BcCSP tethers, and four TmCSP tethers. The folding rates can be described using Arrhenius’s law [Eq. (4)], where BcCSP and TmCSP are along the same curve (solid purple curve) with $k_f^0 = 200 \text{ s}^{-1}$ and the size of folding transition state $l_{ts} = 4.6 \text{ nm}$ and BsCSP (solid black curve) with $k_f^0 = 290 \text{ s}^{-1}$ and the size of folding transition state $l_{ts} = 2.8 \text{ nm}$. The unfolding rates are fitted with Bell’s model to obtain the zero-force unfolding rates and unfolding distances at low forces. Error bar of rates show the standard error of the mean, and force is estimated to have 5% uncertainty.

force, which can be described by:

$$x_{ts}(f) = l_{ts} \coth\left(\frac{fl_{ts}}{k_B T}\right) - \frac{k_B T}{f}, \quad (2)$$

where l_{ts} represents the size of transition state. The force-extension curves of unfolded CSP peptide can be well described by the wormlike chain (WLC) model:

$$\frac{fA}{k_B T} = \frac{x_{\text{chain}}}{L} + \frac{1}{4(1 - x_{\text{chain}}/L)^2} - \frac{1}{4}, \quad (3)$$

where A denotes the persistence length of 0.8 nm, x_{chain} the extension, and L the contour length of the peptide. The force-dependent folding rate can be described by the Arrhenius’s law:

$$k_f(f) = k_f^0 \exp\left[-\int_0^f x_f(f') df' / k_B T\right], \quad (4)$$

where $x_f(f) = x_{\text{chain}}(f) - x_{ts}(f)$ denotes the folding distance. The force-dependent folding rates of BcCSP and TmCSP can be described by a curve with $k_f^0 = 200 \text{ s}^{-1}$ and $l_{ts} = 4.6 \text{ nm}$, while those of BsCSP follows a curve with $k_f^0 = 290 \text{ s}^{-1}$ and $l_{ts} = 2.8 \text{ nm}$ [Fig. 4(d)].

C. Specific force-dependent unfolding rates at large forces

We conducted force-jump experiments to determine the unfolding rates of BsCSP and BcCSP over a wider force range [Figs. 5(a) and 5(b)]. First the force was maintained at 1 pN for a sufficient duration to ensure that the CSP folded to native state. Figure 5(a) illustrates the force-jump cycle of BsCSP, where it undergoes jumps from 1 pN to higher forces ranging from 5 to 10 pN, with a 4-s interval at 1 pN. Due to the rapid unfolding rate of BsCSP, sometimes we cannot detect signals of BsCSP unfolding. Figure 5(b) describes the force-jump cycles of BcCSP from 1 to 8–30 pN, with a 10-s interval. When the force reaches 30 pN, in addition to the unfolding signal of CSP, unzipping-zipping transitions of SpyTag-SpyCatcher can also be observed, providing strong evidence that the tethers are correct [34]. The force jump measurement for TmCSP can be referred to our previous study [28]. Similarly, the unfolding rate k_u in force-jump measurement can be determined by exponential fitting to the survival probability of the native states of CSPs [Figs. 5(c) and 5(d)].

Unfolding step size increases with force. The average step size plus extension of the native state gives the extension of the unfolded polypeptide, which can be fitted with WLC model (Fig. S3) [41].

In Fig. 6(a), we present the unfolding and folding rates of CSPs across the entire range of forces. The unfolding rates

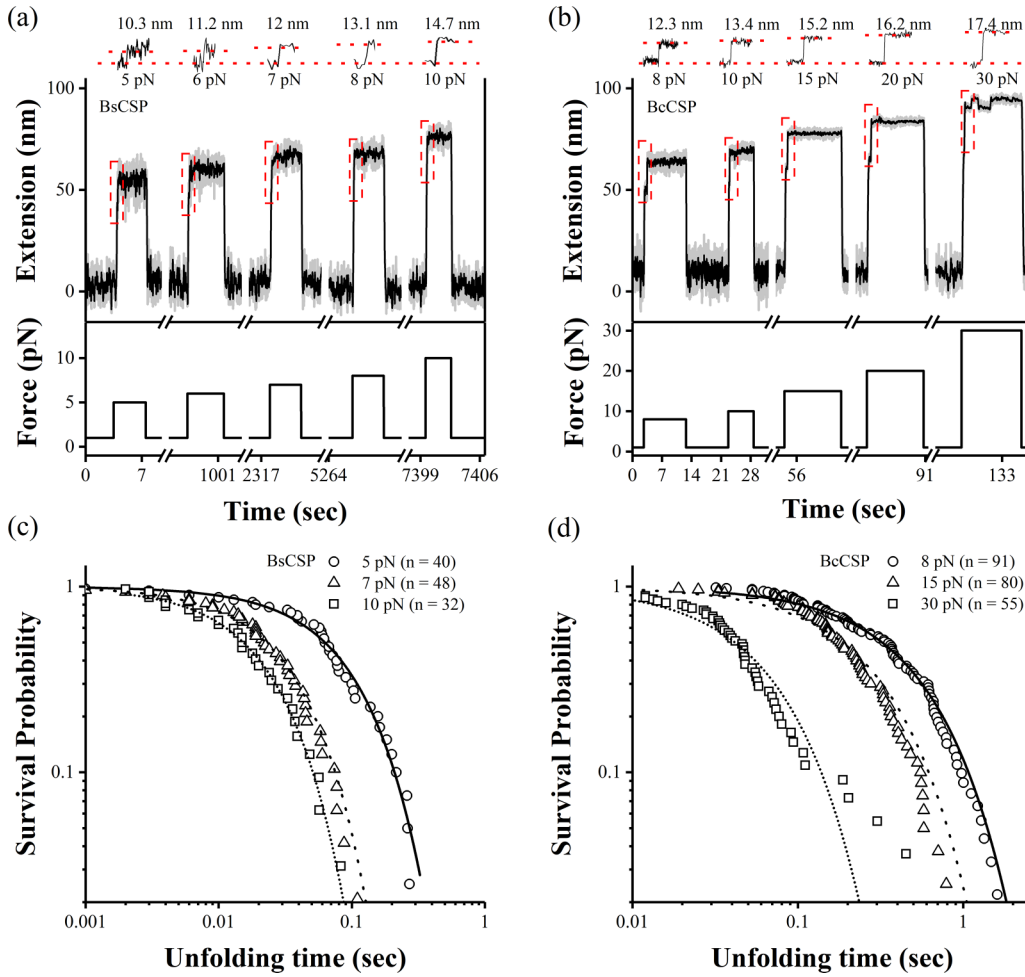


FIG. 5. Unfolding dynamics of BsCSP and BcCSP at different forces measured in the force-jump experiment. Representative force-jump measurement of the unfolding courses of BsCSP at 5 to 10 pN (a) and BcCSP at 8 to 30 pN (b). For BcCSP, unzipping-zipping transitions of SpyTag-SpyCatcher can be observed at 30 pN. Raw data were recorded at 200 Hz (gray) and smoothed in a time window of 0.1 s (black). (c) The survival probability of the native state of BsCSP at 5, 7, and 10 pN. (d) The survival probability of the native state of BcCSP at 8, 15, and 30 pN. The data in (c) and (d) are from three independent BsCSP, and BcCSP protein tethers. Straight lines correspond to single exponential fitting results.

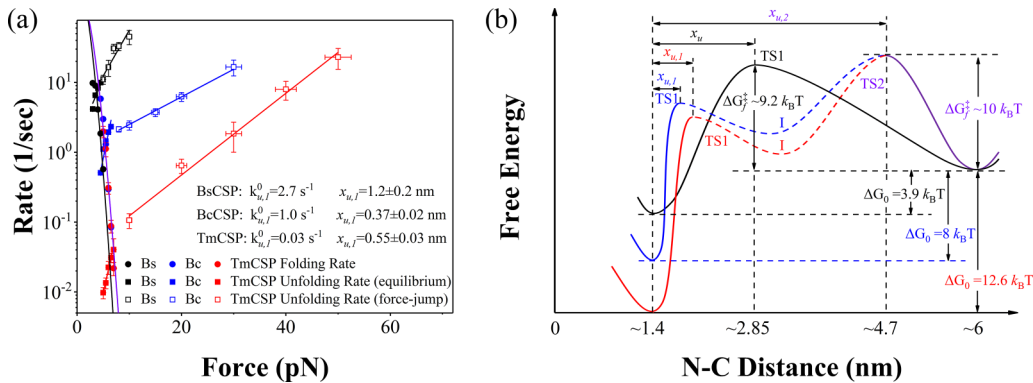


FIG. 6. Force-dependent unfolding and folding rates and free-energy landscape of CSPs. (a) The unfolding and folding rates obtained from the equilibrium measurements (solid symbols) and force-jump measurements (open symbols) for three CSPs. The average unfolding rates were obtained from force-jump measurements for three BsCSP, BcCSP, and four TmCSP protein tethers. Error bar of rates show the standard error of the mean, and force is estimated to have 5% uncertainty. The unfolding rates of BsCSP at 5–10 pN (black line), BcCSP at 8–30 pN (blue line), and TmCSP at 10–50 pN (red line, refer to our previous study) are fitted with Bell’s model to determine $k_{u,1}^0$ and $x_{u,1}$. (b) Using unfolded states of BsCSP, BcCSP, and TmCSP as the reference, and the free-energy landscapes of all three CSPs are constructed from folding free energy, barrier height, and location of TS1 and TS2. The dashed lines between TS1 and TS2 represent transient intermediate states which may exist but cannot be directly observed in magnetic tweezers experiments.

follow the trend BsCSP>BcCSP>TmCSP at the same force. The significant difference in stability is primarily reflected in the unfolding rate rather than the folding rate, which aligns with previous biochemical studies [25].

To verify that the different slopes observed in the unfolding rate across different force intervals are not due to the use of different measurement methods (constant force vs force-jump experiments), we conducted force jump experiments on BcCSP at forces of 5 and 6 pN. The results obtained from these experiments were consistent with the findings from constant force experiments (Fig. S4) [41].

We utilized the Bell's model to fit the high-force unfolding rates (fitting parameters with subscript "1"). The unfolding rates of BsCSP from 5 to 10 pN give $k_{u,1}^0 = 2.7 \pm 1.1 \text{ s}^{-1}$ and $x_{u,1} = 1.2 \pm 0.2 \text{ nm}$. Similarly, fitting of the unfolding rates of BcCSP from 8 to 30 pN gives $k_{u,1}^0 = 1.0 \pm 0.1 \text{ s}^{-1}$ and $x_{u,1} = 0.37 \pm 0.02 \text{ nm}$. Additionally, as described in previous studies [28], unfolding rates of TmCSP ranging from 10 to 50 pN give $k_{u,1}^0 = (3.0 \pm 0.7) \times 10^{-2} \text{ s}^{-1}$ and $x_{u,1} = 0.55 \pm 0.03 \text{ nm}$. These large force unfolding distances of CSPs do not exhibit any discernible consistency.

D. Common and specific features of free-energy landscapes of BsCSP, BcCSP, and TmCSP

With the force-dependent folding-unfolding rates and the critical force, the free-energy landscape of protein can be constructed. The protein folding free energy $\Delta G_0 = \int_0^{f_c} \Delta x(f') df'$, where Δx is force-dependent unfolding step size (Fig. S3) [41]. ΔG_0 is $3.9 k_B T$ for BsCSP, $8.0 k_B T$ for BcCSP, and $12.6 k_B T$ for TmCSP. Comparing with the biochemical experiment ΔG_0 values [25], ΔG_0 of BsCSP is slightly smaller than the biochemical measurement values ($4.1\text{--}4.7 k_B T$), ΔG_0 of BcCSP matches the biochemical measurement values ($7.4\text{--}9.4 k_B T$), and ΔG_0 of TmCSP is slightly larger than the biochemical measurement values ($9.9\text{--}12.4 k_B T$). Therefore, ΔG_0 of BsCSP, BcCSP, and TmCSP is approximately consistent with previous biochemical studies.

For BcCSP and TmCSP, the low-force $x_{u,2}$ is much greater than the high-force $x_{u,1}$ by more than six times, which indicates that there are two separate free-energy barriers along the unfolding pathway. However, for BsCSP, the low-force $x_{u,2}$ and high-force $x_{u,1}$ differs by only 0.5 nm which is equal to the summation of errors of $x_{u,1}$ and $x_{u,2}$, indicating that there is only one merged wide barrier along the unfolding pathway. The crystal structures of three CSPs reveal similar distances between the N- and C-termini, typically around 1.4 nm. For BsCSP, $x_{u,1} = 1.2 \pm 0.2 \text{ nm}$ and $x_{u,2} = 1.7 \pm 0.3 \text{ nm}$ give the one transition state at about 2.85 nm. BcCSP exhibits two transition states located at 1.77 nm (TS1) and 4.9 nm (TS2), respectively. Consistent with our previous work, TmCSP has two transition states located at 1.95 nm (TS1) and 4.5 nm (TS2), respectively [28]. Considering the acceptable margin of error, the TS2 for the BcCSP and TmCSP can be consolidated to a common barrier with size of about 4.7 nm.

To calculate the free energy of the transition states, we made an assumption that the intrinsic conformation relaxation rate of a small protein, denoted as k^* , is 10^6 s^{-1} . The free energy of the transition state, ΔG^\ddagger , can be determined with $k_u^0 = k^* \exp(-\Delta G^\ddagger/k_B T)$. Then, the estimated unfolding

barriers of BsCSP are $12.8 k_B T$ and $13.4 k_B T$, which gives an average unfolding barrier of $13.1 k_B T$. For BcCSP, the unfolding barriers are estimated to be $13.8 k_B T$ (TS1) and $18.4 k_B T$ (TS2). For TmCSP, the unfolding barriers are estimated to be $17.2 k_B T$ (TS1) and $22.1 k_B T$ (TS2), referring to our previous study [28]. Although not directly observed in our experiment due to limited resolution of our magnetic tweezers, we assume the existence of a transient intermediate state (I) between separated TS1 and TS2 of BcCSP and TmCSP.

By using the unfolded state as the reference with zero free energy, the free-energy landscapes of BsCSP, BcCSP, and TmCSP are plotted using the N-C distance as the reaction coordinate [Fig. 6(b)]. Since BcCSP and TmCSP exhibit the same force-dependent folding rates at low force and similar $x_{u,2}$, they share a common free-energy barrier TS2, while TS1 for each CSP is specific. Theoretically the extension is zero without stretching force. We approximate the N-C distances of the transition states as their extensions with stretching force. N-C distance of the unfolded state is estimated to be around 6 nm based on polymer model of the polypeptide chain.

IV. DISCUSSION

In this study, we utilized magnetic tweezers to measure the force-dependent folding and unfolding rates of three homologous CSP proteins with tremendous different thermal stability in force range from several pN to tens of pN. The force-dependent folding dynamics of CSPs are similar, which demonstrates that the folding dynamics is mainly determined by the topological structure of their native states, rather than the intricate interactions between specific amino acids. On the other hand, the force-dependent unfolding rates of BsCSP, BcCSP, and TmCSP decrease sequentially by roughly one to two orders of magnitude, despite their similar folding dynamics. Therefore, the large difference in thermal stability is mainly from their distinguished unfolding rates.

From force-dependent folding and unfolding rates, free-energy landscapes of CSPs are constructed [Fig. 6(b)]. Both BcCSP and TmCSP are stable with folding free energy greater than eight $k_B T$. There are two unfolding barriers, with one barrier (TS1) dominant at high force and another one (TS2) dominant at low force. The possible intermediate state I between TS1 and TS2 are not directly recorded in both equilibrium measurements and force-jump experiments, which might be due to its short lifetime during the transitions. Additionally, the identical folding dynamics and similar unfolding distances $x_{u,2}$ of BcCSP and TmCSP indicate that the transition state TS2 is their common primary barrier at low forces.

In contrast to BcCSP and TmCSP, BsCSP has the lowest thermal stability with ΔG_0 of only $3.9 k_B T$, a little bit smaller folding rate, and the largest unfolding rate. We can only measure its unfolding rate in force range of 3–10 pN. With that, the reconstructed free-energy landscape of BsCSP shows one barrier with size in between TS1 and TS2 of BcCSP and TmCSP.

The slopes of the logarithm of the unfolding rate as functions of force are different at the high force regime. Fitting with Bell's model gives distinct unfolding distances of 1.2 ± 0.2 , 0.37 ± 0.02 , and $0.55 \pm 0.03 \text{ nm}$ for BsCSP, BcCSP, and TmCSP, respectively. This shows that the locations of

transition state TS1 are protein specific, which indicates that the destroyed interactions in TS1 depends on the specific interactions in the native state of each CSP protein. The obtained unfolding distance of 1.2 nm for BsCSP by magnetic tweezers has discrepancy with the previous results of 0.45 nm by AFM experiments [36], which might be due to the different force range of the measurements (5–10 pN for magnetic tweezers experiments and 40–80 pN for AFM experiments).

In our study we construct the free-energy landscape mainly based on the folding free energy determined from equilibrium measurement and the force-dependent unfolding rates. If only nonequilibrium measurements can be done, then the folding free energy can also be obtained by Jarzynski equation or Crooks theorem [37–39], which need lots of measurements to get an accurate mean value or intersection point of the work done in folding and unfolding transitions. Another method to construct the free-energy landscape from equilibrium measurement is using the Boltzmann relation of the free energy with the distribution of extension [40]. But it requires

both high-resolution measurement and complicated deconvolution procedure which are not easy to achieve by our magnetic tweezers.

CSP has the ability to bind single-stranded nucleic acids, disrupting the secondary structures of RNA that might form on temperature drop, thereby facilitating normal protein expression in living organisms. The interaction between CSP and single-stranded nucleic acids needs further investigation to provide valuable insights into the molecular mechanism of the physiological function of CSPs.

ACKNOWLEDGMENTS

This work was supported by the National Natural Science Foundation of China (Grants No. 12174322 to H.C., No. 12204124 to Z.G., and No. 32271367 and No. 12204389 to S.L.), 111 project (B16029), and research grant from Wenzhou Institute.

-
- [1] J. Wang and E. Panagiotou, The protein folding rate and the geometry and topology of the native state, *Sci. Rep.* **12**, 6384 (2022).
- [2] E. J. Miller, K. F. Fischer, and S. Marqusee, Experimental evaluation of topological parameters determining protein-folding rates, *Proc. Natl. Acad. Sci. USA* **99**, 10359 (2002).
- [3] E. Alm and D. Baker, Prediction of protein-folding mechanisms from free-energy landscapes derived from native structures, *Proc. Natl. Acad. Sci. USA* **96**, 11305 (1999).
- [4] E. Alm and D. Baker, Matching theory and experiment in protein folding, *Curr. Opin. Struct. Biol.* **9**, 189 (1999).
- [5] V. Ulyanova, A. Nadyrova, E. Dudkina, A. Kuznetsova, A. Ahmetgalieva, D. Faizullin, Y. Surchenko, D. Novopashina, Y. Zuev, N. Kuznetsov, and O. Ilinskaya, Structural and functional differences between homologous bacterial ribonucleases, *Int. J. Mol. Sci.* **23**, 1867 (2022).
- [6] D. R. Tompa, M. M. Gromiha, and K. Saraboji, Contribution of main chain and side chain atoms and their locations to the stability of thermophilic proteins, *J. Mol. Graphics Modell.* **64**, 85 (2016).
- [7] H. X. Zhou and F. Dong, Electrostatic contributions to the stability of a thermophilic cold shock protein, *Biophys. J.* **84**, 2216 (2003).
- [8] S. A. Wells, S. J. Crennell, and M. J. Danson, Structures of mesophilic and extremophilic citrate synthases reveal rigidity and flexibility for function, *Proteins* **82**, 2657 (2014).
- [9] T. B. Mamonova, A. V. Glyakina, O. V. Galzitskaya, and M. G. Kurnikova, Stability and rigidity/flexibility—two sides of the same coin?, *Biochim. Biophys. Acta.* **1834**, 854 (2013).
- [10] C.-H. Chan, C. C. Wilbanks, G. I. Makhatadze, and K.-B. Wong, Electrostatic contribution of surface charge residues to the stability of a thermophilic protein: Benchmarking experimental and predicted pKa values, *PLoS One* **7**, e30296 (2012).
- [11] M. Robinson-Rechavi, A. Alibés, and A. Godzik, Contribution of electrostatic interactions, compactness and quaternary structure to protein thermostability: Lessons from structural genomics of *Thermotoga maritima*, *J. Mol. Biol.* **356**, 547 (2006).
- [12] U. D. Priyakumar, S. Ramakrishna, K. R. Nagarjuna, and S. K. Reddy, Structural and energetic determinants of thermal stability and hierarchical unfolding pathways of hyperthermophilic proteins, *Sac7d* and *Sso7d*, *J. Phys. Chem. B* **114**, 1707 (2010).
- [13] M. Sadeghi, H. Naderi-Manesh, M. Zarrabi, and B. Ranjbar, Effective factors in thermostability of thermophilic proteins, *Biophys. Chem.* **119**, 256 (2006).
- [14] M. M. Gromiha, M. C. Pathak, K. Saraboji, E. A. Ortlund, and E. A. Gaucher, Hydrophobic environment is a key factor for the stability of thermophilic proteins, *Proteins* **81**, 715 (2013).
- [15] U. D. Priyakumar, Role of hydrophobic core on the thermal stability of proteins—Molecular dynamics simulations on a single point mutant of *Sso7d* abstract, *J. Biomol. Struct. Dyn.* **29**, 961 (2012).
- [16] P. L. Wintrod, D. Zhang, N. Vaidehi, F. H. Arnold, and W. A. Goddard, Protein dynamics in a family of laboratory evolved thermophilic enzymes, *J. Mol. Biol.* **327**, 745 (2003).
- [17] T. Lazaridis, I. Lee, and M. Karplus, Dynamics and unfolding pathways of a hyperthermophilic and a mesophilic rubredoxin, *Protein. Sci.* **6**, 2589 (1997).
- [18] H. A. Thieringer, P. G. Jones, and M. Inouye, Cold shock and adaptation, *BioEssays* **20**, 49 (1998).
- [19] H. Schindelin, M. A. Marahiel, and U. Heinemann, Universal nucleic acid-binding domain revealed by crystal structure of the *B. subtilis* major cold-shock protein, *Nature (London)* **364**, 164 (1993).
- [20] K. Sasaki, M. H. Kim, and R. Imai, Arabidopsis cold shock domain protein 2 is a negative regulator of cold acclimation, *New. Phytol.* **198**, 95 (2013).
- [21] A. Mani and D. K. Gupta, Single-stranded nucleic acid binding in Arabidopsis thaliana cold shock protein is cold shock domain dependent, *J. Biomol. Struct. Dyn.* **33**, 861 (2015).
- [22] B. N. Dominy, D. Perl, F. X. Schmid, and C. L. Brooks, The effects of ionic strength on protein stability: The cold shock protein family, *J. Mol. Biol.* **319**, 541 (2002).
- [23] P. L. Graumann and M. A. Marahiel, A superfamily of proteins that contain the cold-shock domain, *Trends. Biochem. Sci.* **23**, 286 (1998).

- [24] G. Horn, R. Hofweber, W. Kremer, and H. R. Kalbitzer, Structure and function of bacterial cold shock proteins, *Cell. Mol. Life Sci.* **64**, 1457 (2007).
- [25] D. Perl, C. Welker, T. Schindler, K. Schröder, M. A. Marahiel, R. Jaenicke, and F. X. Schmid, Conservation of rapid two-state folding in mesophilic, thermophilic and hyperthermophilic cold shock proteins, *Nat. Struct. Biol.* **5**, 229 (1998).
- [26] T. Hoffmann, K. M. Tych, D. J. Brockwell, and L. Dougan, Single-molecule force spectroscopy identifies a small cold shock protein as being mechanically robust, *J. Phys. Chem. B* **117**, 1819 (2013).
- [27] J. Schönfelder, R. Perez-Jimenez, and V. Muñoz, A simple two-state protein unfolds mechanically via multiple heterogeneous pathways at single-molecule resolution, *Nat. Commun.* **7**, 11777 (2016).
- [28] H. Hong, Z. Guo, H. Sun, P. Yu, H. Su, X. Ma, and H. Chen, Two energy barriers and a transient intermediate state determine the unfolding and folding dynamics of cold shock protein, *Commun. Chem.* **4**, 156 (2021).
- [29] H. Chen, H. Fu, X. Zhu, P. Cong, F. Nakamura, and J. Yan, Improved high-force magnetic tweezers for stretching and refolding of proteins and short DNA, *Biophys. J.* **100**, 517 (2011).
- [30] H. Chen, G. Yuan, R. S. Winardhi, M. Yao, I. Popa, J. M. Fernandez, and J. Yan, Dynamics of equilibrium folding and unfolding transitions of titin immunoglobulin domain under constant forces, *J. Am. Chem. Soc.* **137**, 3540 (2015).
- [31] R. Tapia-Rojo, E. C. Eckels, and J. M. Fernández, Ephemeral states in protein folding under force captured with a magnetic tweezers design, *Proc. Natl. Acad. Sci. USA* **116**, 7873 (2019).
- [32] Z. Guo, H. Hong, G. Yuan, H. Qian, B. Li, Y. Cao, W. Wang, C. X. Wu, and H. Chen, Hidden intermediate state and second pathway determining folding and unfolding dynamics of GB1 protein at low forces, *Phys. Rev. Lett.* **125**, 198101 (2020).
- [33] H. Sun, Z. Guo, H. Hong, Z. Zhang, Y. Zhang, Y. Wang, S. Le, and H. Chen, Free energy landscape of type III fibronectin domain with identified intermediate state and hierarchical symmetry, *Phys. Rev. Lett.* **131**, 218402 (2023).
- [34] Z. Guo, H. Hong, H. Sun, X. Zhang, C. X. Wu, B. Li, Y. Cao, and H. Chen, SpyTag/SpyCatcher tether as a fingerprint and force marker in single-molecule force spectroscopy experiments, *Nanoscale* **13**, 11262 (2021).
- [35] B. Zakeri, J. O. Fierer, E. Celik, E. C. Chittock, U. Schwarz-Linek, V. T. Moy, and M. Howarth, Peptide tag forming a rapid covalent bond to a protein, through engineering a bacterial adhesin, *Proc. Natl. Acad. Sci. USA* **109**, E690 (2012).
- [36] K. M. Tych, M. Batchelor, T. Hoffmann, M. C. Wilson, E. Paci, D. J. Brockwell, and L. Dougan, Tuning protein mechanics through an ionic cluster graft from an extremophilic protein, *Soft. Matter* **12**, 2688 (2016).
- [37] C. Jarzynski, Nonequilibrium equality for free energy differences, *Phys. Rev. Lett.* **78**, 2690 (1997).
- [38] G. E. Crooks, Entropy production fluctuation theorem and the nonequilibrium work relation for free energy differences, *Phys. Rev. E* **60**, 2721 (1999).
- [39] D. Collin, F. Ritort, C. Jarzynski, S. B. Smith, I. Tinoco, and C. Bustamante, Verification of the Crooks fluctuation theorem and recovery of RNA folding free energies, *Nature (London)* **437**, 231 (2005).
- [40] J. C. Gebhardt, T. gl, and M. Rief, Full distance-resolved folding energy landscape of one single protein molecule, *Proc. Natl. Acad. Sci. USA* **107**, 2013 (2010).
- [41] See Supplemental Material at <http://link.aps.org/supplemental/10.1103/PhysRevResearch.6.023170> for magnetic tweezers setup and force calibration and Figs. S1–S4.